

# Reynolds number scaling of influence of boundary layers on the global behavior of laboratory quasi-Keplerian flows

Eric M. Edlund\* and Hantao Ji  
Princeton Plasma Physics Laboratory

September 1, 2015

## Abstract

We present measurements of quasi-Keplerian flows in a Taylor-Couette device that identify the boundary conditions required to generate near-ideal flows that exhibit self-similarity under scaling of the Reynolds number. These experiments are contrasted with alternate boundary configurations that result in flows that progressively deviate from ideal Couette rotation as the Reynolds number is increased. These behaviors are quantitatively explained in terms of the tendency to generate global Ekman circulation and the balance of angular momentum fluxes through the axial and radial boundary layers.

\*current email address: eedlund@mit.edu

# 1 Introduction

That the global properties of an extended system may be mapped to the boundaries is an idea that has found success in holographic theories of general relativistic systems [1, 2], and in magnetically confined plasmas [3, 4]. We report on a similar behavior observed in incompressible hydrodynamic flows in a Taylor-Couette apparatus where it is observed that certain characteristics of the global flow are largely dictated by the boundaries. This finding is particularly relevant for experiments that examine quasi-Keplerian (QK) flows, that is, rotation satisfying  $0 < q < 2$  where  $q = -d \ln \Omega / d \ln r$ ,  $\Omega$  is the fluid angular velocity and  $r$  is the radial coordinate, as models of astrophysical systems, namely accretion disks. Numerous recent studies have commented on the hydrodynamic stability of such systems [5, 6, 7, 8], with extensions to magnetohydrodynamics in electrically conducting fluids [9, 10, 11, 12, 13].

While there is some disagreement between studies as to whether hydrodynamic turbulence can be induced in QK flows, the balance seems to lean toward the negative, at least insofar as incompressible turbulence is considered, and points to the important role of magnetohydrodynamic effects in astrophysical systems. However, while it is known that QK flows are linearly stable it remains unknown whether there exists a nonlinear transition to turbulence, even for incompressible hydrodynamic systems. Some experiments [5, 6, 7] and simulations [14] indicate that such a transition is not likely, while others present evidence that suggests that a subcritical transition may exist [8] and some simulations find significant transient growth of perturbations that may allow for nonlinear effects to enter [15]. Fluid experiments in other regimes of operation that are not astrophysically-relevant have observed bi-stability [16, 17], suggesting that should a similar mechanism exist for QK systems then a subcritical pathway to turbulence may explain angular momentum transport in accretion disks [18]. We show in this work that the influence of the boundaries is intimately connected to the global structure of flows in Taylor-Couette experiments and, by extension, is also related to the tendency of these systems to generate and sustain turbulence.

One of the long-standing challenges of Taylor-Couette experiments in the quest to understand angular momentum transport in astrophysically-relevant flows has been the parasitic presence of Ekman circulation (secondary circulation) induced by the mismatch between the fluid velocity and the solid body rotation of the axial boundaries. A significant reduction in Ekman circulation has been realized in experiment by using axial boundaries that are split into multiple rings capable of differential rotation. Under particular boundary conditions, azimuthal velocity profiles of the fluid can be generated that very nearly match that of ideal Couette rotation [5, 7, 19, 20], the rotation profile that is expected in the absence of axial influences for a constant radial flux of angular momentum, and has been observed to hold over a wide range of Reynolds numbers [20]. In contrast, studies in the “classical” configuration where the axial boundaries rotate with the outer cylinder have shown performance that further deviates from ideal Couette as the Reynolds number is increased [21]. Such trends are revealing of whether these systems are dominated by boundary interactions or internal dynamics, a distinction with important consequences for the applicability of such experiments to interpretation of astrophysical systems, especially at large Reynolds numbers. First, through the experiments reported here we identify two necessary criteria that define constraints on the boundary configurations that allow near-ideal flows to develop. We then discuss the competing roles of radial (Stewartson) boundary layers and axial (Ekman) boundary layers, from which we develop a model that describes the quantitative departure of the rotation profiles from ideal Couette flow as a function of the angular momentum fluxes through the boundaries.

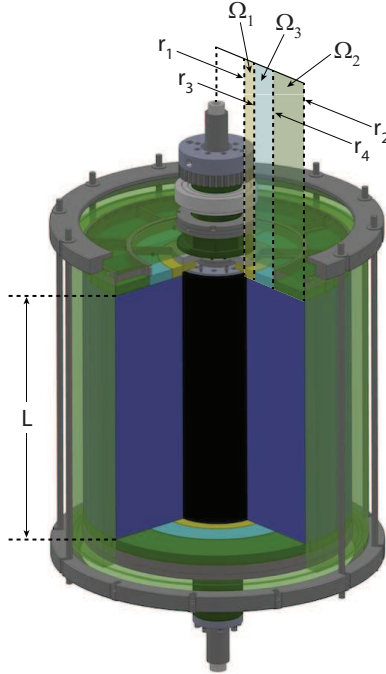


Figure 1: (color online) Illustration of the HTX device at PPPL showing the segmented axial boundaries (yellow, blue and green segments), the inner cylinder in black, the outer cylinder in green and the working fluid in dark blue.

## 2 Experimental Apparatus

A Taylor-Couette (TC) device is a system of coaxial cylinders that rotate independently of each other with the experimental fluid region between. The TC apparatus used in these studies, called the Hydrodynamic Turbulence Experiment (HTX), is a modified version of the classical device in that the axial boundaries in HTX are segmented to allow differential rotation across the boundaries [7]. The inner cylinder radius is  $r_1 = 6.9$  cm and the outer cylinder radius is  $r_2 = 20.3$  cm. The inner radius and outer radius of the independent rings are defined by the parameters  $r_3$  and  $r_4$ , respectively. The axial length of the experimental volume is  $L = 39.8$  cm, giving an aspect ratio of  $\Gamma = L/(r_2 - r_1) = 2.97$  (see Fig. 1). Corresponding components on the top and bottom are driven by the same motor so that the system is up-down symmetric. The angular velocities of the inner cylinder, outer cylinder and rings are identified by  $\Omega_1$ ,  $\Omega_2$  and  $\Omega_3$ , respectively. Rotary encoders report the speed of the motors to the control system.

A laser Doppler velocimeter (LDV) diagnostic system is used to measure the local, azimuthal velocity ( $v_\theta$ ), which in the experiments reported here were measured at the midplane of the device. The LDV system is calibrated by measuring fluid flow in solid body for which, after spin-up, the only velocity component is  $v_\theta$ , which is a unique function of the motor speeds. For these studies we define the global shear Reynolds number as  $\text{Re}_s = r_g^2 \Delta\Omega / \nu$ , where  $r_g = (r_1 r_2)^{1/2}$  is the geometric-mean radius,  $\Delta\Omega = \Omega_1 - \Omega_2$  and  $\nu$  is the kinematic viscosity, approximately  $1 \times 10^{-6}$  m<sup>2</sup>/s for water.

### 3 Observations

The core observation of this work is summarized in Fig. 2, presenting flows under two different values of normalized shear ( $q = 1.8$  and  $q = 1.5$ ) and three different boundary conditions: **Split**, **Optimized**, and **Ekman**. For the  $q = 1.8$  cases these configuration speeds, reported as  $\Omega_1$ - $\Omega_3$ - $\Omega_2$ , are multiples of 350-350-50 RPM (**Split**), 350-185-50 RPM (**Optimized**), and 350-50-50 RPM (**Ekman**). For the  $q = 1.5$  these are 250-250-50 RPM (**Split**), 250-140-50 RPM (**Optimized**), and 250-50-50 RPM (**Ekman**). The reference profile for these studies is described by ideal Couette rotation, defined in terms of angular velocity as  $\Omega_C(r) = \Omega_A + \Omega_B(r_g/r)^2$ , where  $\Omega_A = (r_2^2\Omega_2 - r_1^2\Omega_1)/(r_2^2 - r_1^2)$ ,  $\Omega_B = r_g^2(\Omega_1 - \Omega_2)/(r_2^2 - r_1^2)$ . As a function of azimuthal velocity the Couette solution is  $v_C(r) = r\Omega_C$ . It is interesting that while the **Ekman** and **Split** configurations exhibit progressive departure from ideal Couette as the Reynolds number is increased, the shape of the **Optimized** cases is nearly invariant with respect to scaling of the Reynolds number.

#### 3.1 Necessary conditions for near-ideal flows

Recognizing that the axial boundaries in the **Split** cases will tend to increase the angular momentum flux to the bulk, and conversely for the **Ekman** cases, we begin by considering the ansatz that the balance of angular momentum fluxes across the axial boundaries determines the deviation from ideal Couette. A continuous variation of  $\Omega_3$  from  $\Omega_2$  to  $\Omega_1$  would then suggest that there is some intermediate state for which the profile must pass close to ideal Couette rotation. We now address whether there is a method for predicting this optimal value of  $\Omega_3$ .

The transition between the bulk flow and the walls of the TC device, which may move at very different speeds, occurs over thin boundary layers. The structure of these boundary layers depends on whether we are considering the balance of forces in the axial or radial directions. The bulk flow transitions to the axial boundary speeds over Ekman boundary layers whose thickness scales like  $\delta_E \sim r\text{Re}_b^{-1/2}$ , and in the ideal model of radial boundaries, over Stewartson boundary layers that scale like  $\delta_S \sim r\text{Re}_b^{-1/4}$ , where  $\text{Re}_b = r^2\Omega_b/\nu$  is a local Reynolds number particular to the boundary location  $r$  with boundary speed  $\Omega_b$  [22, 23, 24]. The fluxes of angular momentum across these boundary layers, being inversely proportional to the boundary layer thickness, do not scale proportionally, and hence we anticipate that self-similarity of the global properties need not be preserved as the Reynolds number is scaled. Thus, while the observed variation in the shape of the **Ekman** and **Split** profiles is expected, it comes as some surprise that the **Optimized** profiles are effectively independent of the Reynolds number.

The experiments reported here showed no significant temporal variation in the mean values, hence, it can be stated that in steady-state the net flux of angular momentum into these flows must sum to zero, that is,  $\Phi_1 + \Phi_2 + 2\Phi_z = 0$  where  $\Phi_1$  and  $\Phi_2$  are the fluxes integrated over the inner and outer cylinders, respectively, and  $\Phi_z$  is the axial flux integrated over each axial boundary (with inward towards the fluid defined as a positive flux). The ideal Couette profile is the response to a constant radial flux of angular momentum, implying that  $\Phi_2 = -\Phi_1$  and that the axial fluxes of angular momentum are everywhere zero. Such a state can be imagined in a TC system with free-slip conditions on the axial boundaries, or with a continuously variable boundary that can perfectly match the ideal Couette profile, conditions that will result in vanishing stress at the axial boundaries. The radial flux of angular momentum under these conditions (which we call  $\Phi_C$ , the Couette flux) has a magnitude equal to

$$\Phi_C = \Phi_0 \frac{r_g^2}{r_2^2 - r_1^2} \text{Re}_s, \quad (1)$$

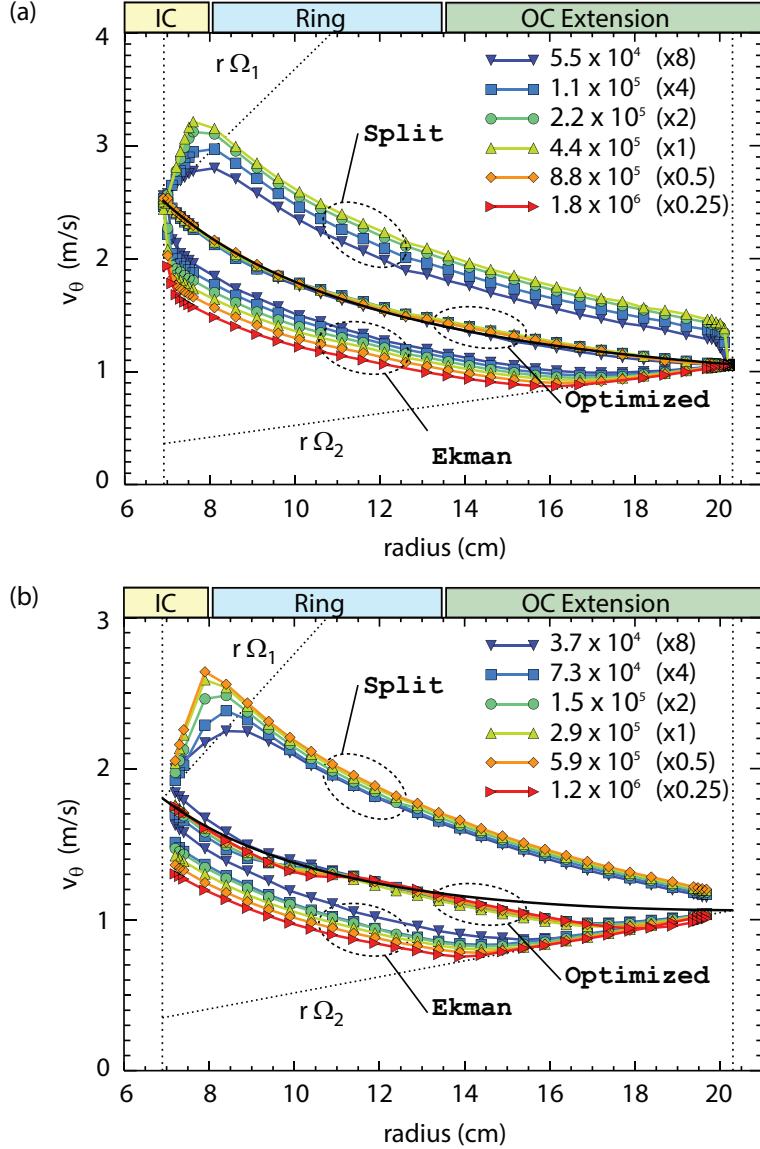


Figure 2: (color online) Scaled measurements of  $v_\theta$  at various  $Re_s$  for (a)  $q = 1.8$  and (b)  $q = 1.5$ .

where  $\Phi_0 = 4\pi\rho\nu^2L$ . As an aside, it is interesting to note that  $\Phi_C = \Phi_0 Re_s$  when the radius ratio ( $r_2/r_1$ ) is equal to the golden ratio.

Even though there is, in general, a large mismatch between fluid and axial boundary speeds, we find that the flows under the **Optimized** boundary conditions very closely approximate the ideal Couette profile, and therefore have a nearly constant radial flux of angular momentum. We now show that rather than satisfying the condition that the axial flux of angular momentum everywhere vanishes, these flows satisfy a much weaker constraint: it is the surface integral of the axial angular momentum flux that vanishes, that is,  $\Phi_z \approx 0$ .

To calculate the axial flux of angular momentum, being proportional to  $d\Omega/dz$ , we make the assumption that  $d\Omega/dz \approx \Delta\Omega_E/\delta_E$ , where  $\Delta\Omega_E = \Omega_b - \Omega$  is the difference of the boundary angular velocity ( $\Omega_b$ ) and the fluid angular velocity just inside the Ekman boundary layer ( $\Omega$ ), and that  $\delta_E = \alpha_E(\nu/\Omega_b)^{1/2}$  represents the thickness of an Ekman boundary layer with an unknown

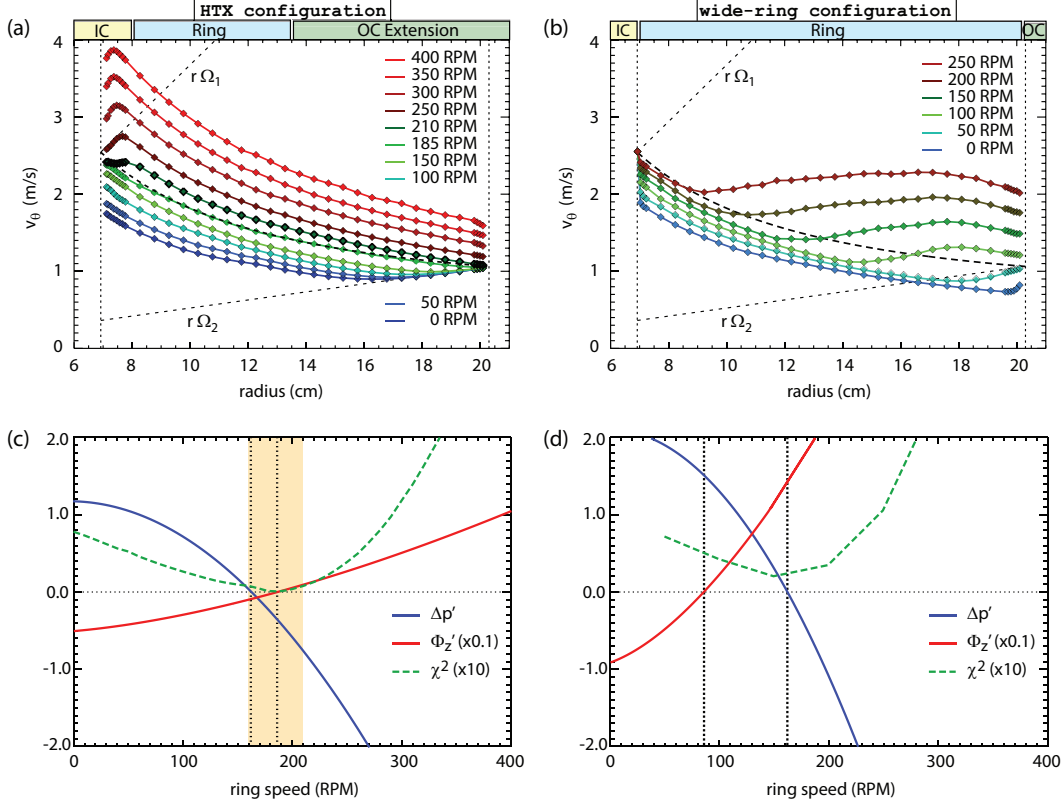


Figure 3: (color online) Experiments conducted in  $q = 1.8$  flows showing  $v_\theta$  as a function of  $\Omega_3$  for the (a) HTX and (b) wide-ring geometries, progressing from low ring speeds (bottom curves) to higher ring speeds (upper curves). In panels (c) and (d) the experimental  $\chi^2$  (dashed green), for the measured profiles relative to the ideal Couette profile for these boundary conditions, is plotted against the calculated axial flux of angular momentum from Eq. 2 (red, increasing function) and the pressure differential from Eq. 3 (blue, decreasing function) for the HTX and wide-ring geometries, respectively.  $\Phi_z$  is normalized by  $\Phi_C$  and  $\Delta p$  is normalized by the kinetic energy density for ideal Couette flow. The vertical dotted lines indicate the zeros of  $\Delta p$  and  $\Phi_z$ .

numerical constant  $\alpha_E$ . Defining the normalized quantities  $\omega = \Omega/\Delta\Omega$  (recalling,  $\Delta\Omega = \Omega_1 - \Omega_2$ ),  $\omega_b = \Omega_b/\Delta\Omega$ ,  $s_1 = r_1/r_g$  and  $s_2 = r_2/r_g$ , we have

$$\Phi_z = \Phi_0 \frac{r_g}{2\alpha_E L} \text{Re}_s^{3/2} \int_{s_1}^{s_2} (\omega_b - \omega) \omega_b^{1/2} s^3 ds. \quad (2)$$

That the radial flux of angular momentum under ideal Couette rotation [Eq. 1] scales like  $\text{Re}_s$ , whereas  $\Phi_z$  scales like  $\text{Re}_s^{3/2}$  means that unless steps are taken to force the integral in Eq. 2 to zero, there will always exist a Reynolds number beyond which the axial flux will overwhelm the Couette flux and cause the flow to depart from ideal rotation, regardless of aspect ratio. From Eq. 2 we can immediately conclude that TC devices of the “classical” geometry with the axial boundaries co-rotating with either the inner cylinder or outer cylinder will always have non-zero  $\Phi_z$  and can therefore never be a good model for astrophysical systems at sufficiently high Reynolds numbers to be of interest. In looking for the conditions under which ideal Couette flow may be generated, we set  $\omega = \omega_C$  and search for the boundary conditions (the  $\omega_b$ ) that cause the integral of Eq. 2 to vanish.

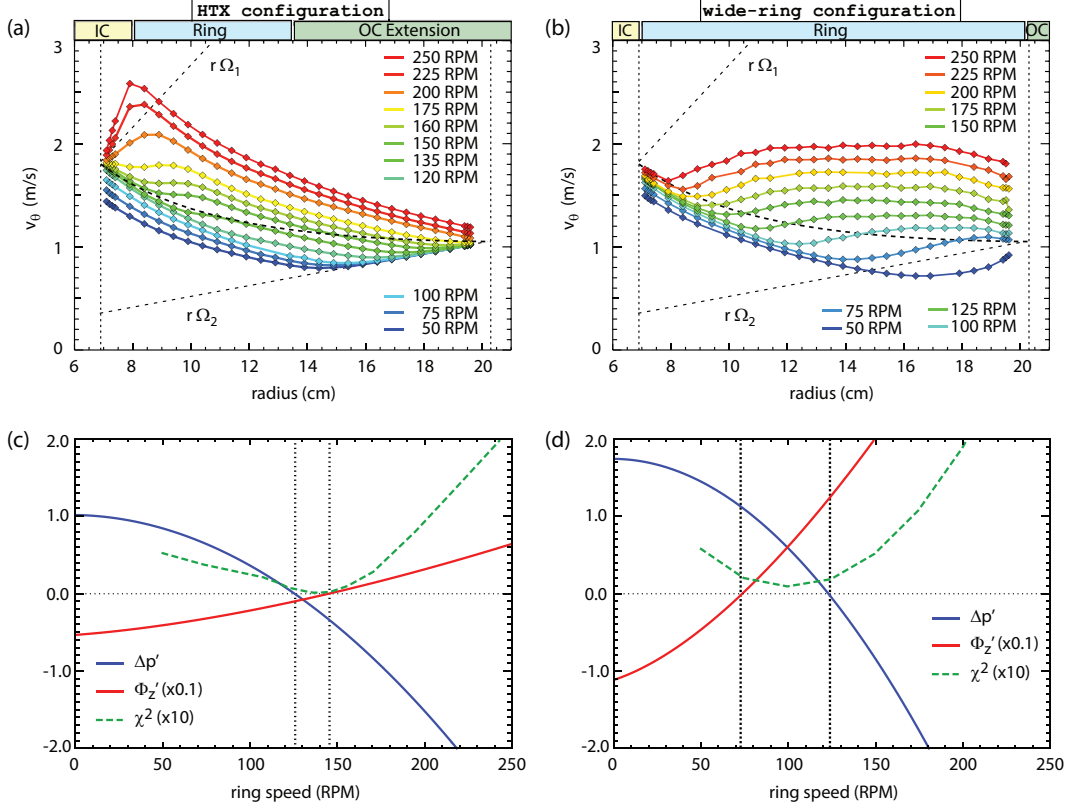


Figure 4: (color online) Same as Fig. 3 except for  $q = 1.5$ .

Figure 3 summarizes fluid velocity measurements over a scan of  $\Omega_3$  for  $q = 1.8$  flows for two axial boundary configurations: the HTX configuration with  $r_3 = 7.8$  cm and  $r_4 = 13.5$  cm, and a **wide-ring** configuration with rings that span the entire radial gap. These experiments show that the HTX configuration produces an exceptional match to the ideal Couette profile for a narrow range of ring speeds centered about 185 RPM, with very low fluctuation levels spanning the entire gap [7]. Importantly, the boundary conditions that generate near-ideal flows for the HTX configuration include the zero crossing of  $\Phi_z$  [Fig. 3(c)]. However, the **wide-ring** case also has a zero in  $\Phi_z$ , near 85 RPM [Fig. 3(d)], yet its flows never resemble ideal Couette, indicating that the vanishing of  $\Phi_z$  is a necessary but not sufficient condition for achieving near-ideal flows.

The role of the axial boundaries in dictating global performance has also been interpreted through the competition of pressures from the bulk flow and from the boundary flow that is viscously coupled to the axial boundaries [25, 26]. The tendency to drive secondary flows was shown to be consistent with whether the bulk pressure is larger than (Ekman circulation) or smaller than (anti-Ekman circulation) the boundary pressure. Following the intuition motivated by these simulations, we define a function  $\Delta p$  that characterizes the average pressure difference between ideal Couette rotation and boundary rotation,

$$\Delta p = \frac{\rho r_g^3 \Delta \Omega^2}{\Delta r} \int_{s_1}^{s_2} \int_{s_1}^s (\omega_C^2 - \omega_b^2) s' ds' ds. \quad (3)$$

For the **wide-ring** configuration the zeros of  $\Delta p$  and  $\Phi_z$  are widely separated, meaning that no circumstance exists where pressure balance and zero net axial flux can be simultaneously satisfied. In contrast, the HTX configuration has zeros of these functions that are nearly coincident

and fall within the operating range in which small fluctuations were observed in Ref. [7]. Other boundary configurations with  $q = 1.5$  also have nearly coincident zeros of  $\Phi_z$  and  $\Delta p$ , in remarkably good agreement with experiments; see Fig. 4. Note that the requirement of coincident or nearly-coincident zeros represents an effective third constraint. These studies suggest that the requirements of having nearly coincident zeros of  $\Phi_z$  and  $\Delta p$  for the generation of ideal flows may represent necessary and sufficient conditions. Additional research conducted over a wider range of geometries and shear conditions will provide a stronger test of this hypothesis.

### 3.2 Departure of flows from ideal Couette

While the coincident vanishing of  $\Phi_z$  and  $\Delta p$  define what may be necessary and sufficient conditions for ideal flows to develop, they do not reveal how QK systems should behave under non-optimized conditions. A general model of the fluid response to forcing by the boundaries must account for the fluxes across both axial and radial boundary layers. As there does not exist a theory of Stewartson boundary layers under the conditions of QK rotation at large Reynolds numbers, we cannot rely on results derived from a linear analysis of perturbative differences in rotational speeds [24], especially for experimental conditions where the Stewartson boundary layers are turbulent [7]. Instead, we assume a generalized scaling of the Stewartson boundary layer thickness of the form  $\delta_S = \alpha_S r (r/L) \text{Re}_b^\beta$ , taking the exponent of the Reynolds number ( $\beta$ ) as a free-parameter to be determined from the observed scalings in Fig. 2. While the numerical factors  $\alpha_E$  and  $\alpha_S$  are introduced through the definitions of the boundary layer thicknesses we cannot measure the boundary layers directly, and therefore we must interpret their meaning as a measure of the effectiveness of angular momentum flux.

We begin this analysis by considering the Ekman configurations from Fig. 2 where we note that  $v_\theta$  transitions to solid body rotation at  $\Omega_2$  near the outer cylinder, implying that  $\Phi_2 \approx 0$ . With a jump in azimuthal velocity (a negative  $\Delta v$ ) occurring over a Stewartson layer at the inner cylinder, the appropriate form for  $\Phi_1$  is

$$\Phi_1 = -\Phi_0 \frac{c_1}{2\alpha_S} \text{Re}_s^\beta \frac{L\Delta v}{\nu}, \quad (4)$$

where  $c_1 = (r_1\Omega_1/r_2\Delta\Omega)^\beta$  is a result of converting from a representation of the boundary layer thickness that depends on the local  $\text{Re}_b$  to a global  $\text{Re}_s$ . We approximate these flows with a piecewise function of the form  $v_\theta(r_a < r < r_t) = v_C + \Delta v$  and  $v_\theta(r_t < r < r_2) = r\Omega_2$ , where  $r_t$  is the transition radius, similar to the identification of separate flow regions in the recent work of Nordsiek *et al.* [21]. Substituting this rotation profile into Eq. 2 (using  $\omega = v_\theta/r\Delta\Omega$ ) and using Eq. 4 for the radial flux at  $r_1$ , we solve the global balance of angular momentum,  $\Phi_1 + 2\Phi_z = 0$ , for the dimensionless  $\Delta v'_{\text{neg}} = \Delta v/r_g\Delta\Omega$  as a function of  $\text{Re}_s$ . Noting that  $\Phi_z$  has two parts given this representation, our solution has three terms and is of the form

$$\Delta v'_{\text{neg}} = \frac{f_1}{\alpha c_1 \frac{L^2}{2r_g^2} \text{Re}_s^{\beta-1/2} + f_2}, \quad (5)$$

where  $\alpha = \alpha_E/\alpha_S$ , and the integral expressions  $f_1$  and  $f_2$  are defined as

$$f_1 = \int_{s_1}^{s_t} (\omega_b - \omega_C) \omega_b^{1/2} s^3 ds \quad (6)$$

$$f_2 = \int_{s_1}^{s_t} \omega_b^{1/2} s^2 ds. \quad (7)$$



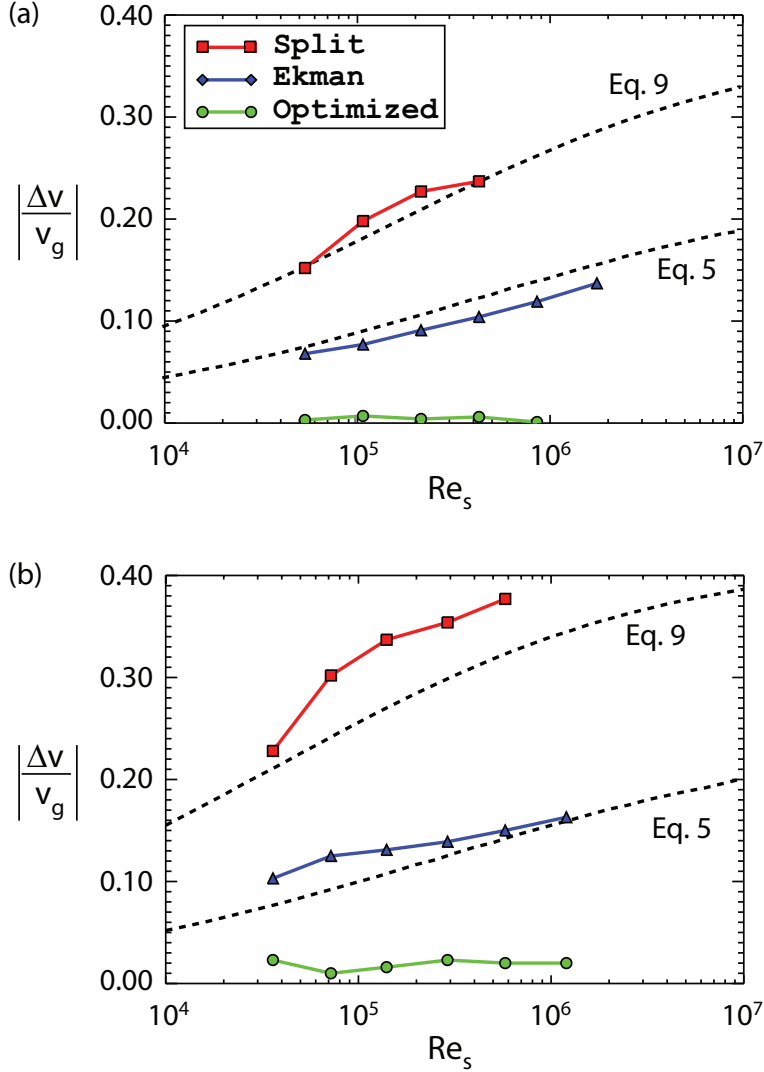


Figure 5: (color online) Scaling of the velocity differential  $\Delta v$  for the three groups of boundary conditions from Fig. 2 for (a)  $q = 1.8$  and (b)  $q = 1.5$ . The dashed lines in the figure are the solutions to Eqs. 5 and 9 with  $\beta = 0.08$  and  $\alpha_E/\alpha_S = 15$ .

Equation 5 is a transcendental expression in  $\Delta v$  since the limits of the integrals in  $f_1$  and  $f_2$  are functions of  $r_t$  which itself depends on  $\Delta v$ . Equation 5 has only two free parameters:  $\beta$  and  $\alpha = \alpha_E/\alpha_S$ . Comparison of Eq. 5 with experimental measurements of  $\Delta v$  is presented in Fig. 5 for the  $q = 1.8$  and  $q = 1.5$  cases, where values of  $\beta \approx 0.08$  and  $\alpha_E/\alpha_S \approx 15$  provide the best fit to the experimental measurements.

This analysis can be extended to the case of the Split configuration with positive  $\Delta v$  by accounting for the different boundary conditions and a slightly more complex flow structure. The most important feature of the positive  $\Delta v$  cases is that there is a nearly linear decrease in  $\Delta v$  across the gap, where  $\Delta v$  at  $r_2$  is defined to be equal to  $\epsilon \Delta v$ . In the  $q = 1.8$  cases  $\Delta v$  decreases by about 60% across the gap ( $\epsilon = 0.4$ ), and by 80% for  $q = 1.5$  ( $\epsilon = 0.2$ ), nearly independent of Reynolds number. The radial flux at  $r_2$  in terms of the  $\epsilon$  reduced  $\Delta v$  is

$$\Phi_2 = \Phi_0 \frac{c_2}{2\alpha_S} \text{Re}_s^\beta \frac{L \epsilon \Delta v}{\nu}, \quad (8)$$

where  $c_2 = (r_2 \Omega_2 / r_1 \Delta \Omega)^\beta$ . The solution for positive, normalized  $\Delta v$  is

$$\Delta v'_{pos} = \frac{f_3}{\epsilon \alpha c_2 \frac{L^2}{2r_g^2} \text{Re}_s^{\beta-1/2} + f_4}, \quad (9)$$

where, similar to Eq. 5, we have

$$f_3 = \int_{s_t}^{s_2} (\omega_b - \omega_C) \omega_b^{1/2} s^3 ds \quad (10)$$

$$f_4 = \int_{s_t}^{s_2} \left[ \frac{s_2 - \epsilon s_t - (1 - \epsilon)s}{s_2 - t} \right] \omega_b^{1/2} s^2 ds. \quad (11)$$

For the **Split** cases, the term  $s_t$  defines the transition point from increasing to decreasing  $\Delta v$ , and the terms in square brackets in Eq.11 derive from the variation of  $\Delta v$  with radius (note that if  $\Delta v$  were constant across the gap then  $\epsilon = 1$  and the term in brackets reduces to unity, recovering Eq. 7). Equation 9 is compared against the measured  $\Delta v'$  in Fig. 5 and is also found also to be in good agreement with experiment when using the same values of  $\alpha_E/\alpha_S$  and  $\beta$  derived from the analysis of the **Ekman** cases.

The success of this model in reproducing the general features of the departures from ideal Couette is remarkable given that it represents a simple accounting of the angular momentum fluxes across the boundaries, ignoring completely the complex internal dynamics of these flows, especially at large Reynolds number where a substantial fraction of the volume exhibits turbulent fluctuations [7]. What disagreement exists between experiment and theory should not overshadow the success of this model in reproducing the general trend of the velocity deviations, the relative amplitude of the positive and negative  $\Delta v$  cases, and the change in the amplitude of the positive  $\Delta v$  cases between  $q = 1.8$  and  $q = 1.5$ . While the model presented here uses a single set of parameters for both values of  $q$ , better fits to the data can be found if we let these parameters depend on  $q$ . It is also possible the these parameters may depend on geometry and Reynolds number in a way that is not captured by the power-law scaling used here.

Studies of the measured fluctuation levels arising from the Stewartson boundary layers in Ref. [7] found that the transition to turbulent Stewartson boundary layers was consistent with the Taylor model of low Reynolds number centrifugal instability. So while cannot offer a precise explanation for why  $\beta$  should take a value close to 0.1, we reiterate that the inferred scaling applies to the angular momentum flux which is a combination of variations in the boundary layer thickness and an effective viscosity within these layers that is modified by turbulent fluctuations. It is beyond the scope and ability of these experiments to identify the separate scalings of the turbulent viscosity and the thickness of the Stewartson boundary layers, though perhaps future experiments will be able to provide greater insight into this problem.

## 4 Conclusions

We conclude with an outlook to future physical and numerical experiments. The ratio of  $\Phi_z$  and  $\Phi_C$  explored earlier can be recast as a constraint on the aspect ratio  $L/\Delta r$  as a function of the Reynolds number. The relative contribution of  $\Phi_z$  can be made arbitrarily small by increasing the axial size of the system, so that to make  $\Phi_z/\Phi_C \approx 10^{-2}$  for an **Ekman** configuration, for example, one would

need an aspect ratio of order 100 at a Reynolds number of  $10^6$ . Outside of using very large aspect ratios, one can employ mechanical advantages as we have done in HTX, such as extensions of the inner and outer cylinder or independent rings. Despite the desire to simplify the mechanical design of such modified TC devices, further analysis shows that the only way to achieve simultaneous zeros in  $\Phi_z$  and  $\Delta p$  is through a design with at least one independent ring. Greater insight into the balance of forces in quasi-epplerian flows could be explored in future experiments in modified Taylor Couette devices like HTX. In particular, further exploration of the Reynolds number dependence on these deviations, the dependence of the model parameters on  $q$ , and the structure of the Ekman cells would tell us much more about the influence of the boundaries on global behavior.

We have shown that nearly ideal flows exhibit profile shape invariance under scaling of the Reynolds number, an effect we interpret through the dual conditions of vanishing axial angular momentum flux and vanishing pressure differential that are nearly simultaneously satisfied, offering predictive capability for selecting optimized boundary conditions and in experimental design. The strongest piece of evidence in support of this model is the prediction of self-similarity of the profiles with respect to scaling of the Reynolds number only for cases in which the axial flux of angular momentum and the pressure differential vanish nearly coincidentally, a prediction in excellent agreement with the observations presented in Fig. 2. It should be reiterated that while the experiments for **Optimized** flows show very small departures from ideal Couette, and whose interpretation is congruent with the coincident zeros in  $\Delta p$  and  $\Phi_z$ , this does not strictly prove that these criteria represent true sufficient conditions. An interesting problem for future studies would be to measure how the departures from ideal Couette depend on the “distance” between these zeros.

It is interesting to note that in all cases presented here the local axial fluxes of angular momentum may be quite large given the substantial difference in speed between the bulk fluid and the axial boundaries, and that it is only on summation over the axial boundaries that zero net axial flux is realized for the **Optimized** cases. Recalling that multiple experiments [7, 20, 19] and simulations [25, 27] have observed a nearly uniform axial structure through the bulk of the fluid volume, the existence of the large axial fluxes naturally raises the question: What allows the bulk flows to depart from the solid body rotation forced by the boundaries? Intuition based on the Taylor-Proudman theorem for Rayleigh-stable flows, that is  $dv_\theta/dz \approx 0$ , would suggest that the bulk should tend to follow the boundary. However, it should be recalled that the Ekman boundary layers do not need to satisfy the Taylor-Proudman theorem because the axial gradient of  $v_\theta$  is balanced with a viscous diffusion of vorticity over the scale of the boundary layer thickness. Thus, the nearly uniform axial structure suggests that the large fluxes of angular momentum that must be present due to the existence of the Ekman boundary layers are redistributed locally, perhaps by small Ekman cells that do not extend far into the bulk of the fluid or even in the boundary layers themselves. As has been shown in prior studies, the free-shear layer that develops at the interface between the differentially rotating rings on the axial boundaries is expected to be centrifugally unstable and may help to enhance the redistribution of angular momentum locally [13].

Another problem for future experiments, both physical and numerical, will be to explore in greater detail how the very large, local fluxes of angular momentum are redistributed near the axial boundaries with only minor effect on the bulk flow in the **Optimized** configurations. Non-optimized boundaries, like the **Split** and **Ekman** configurations, show progressive departure from the ideal Couette flow as the Reynolds number is increased, in agreement with the expectations of a dominant axial flux of angular momentum. A good test for numerical experiments will be to accurately model the global behavior of the mean flows in TC experiments by properly accounting for the angular momentum fluxes from the boundaries. We believe that the boundary layer scalings presented here may enable simulations to bootstrap to larger effective Reynolds numbers by using

specified boundary flux models, thus bypassing the need for very fine grids to resolve the boundary layer structure directly. With the combination of recent simulations of QK flows that can attain Reynolds numbers of the order of  $10^5$  [14, 28], though with axially-periodic boundary conditions, a specified-flux boundary model may allow simulations to reach something resembling experimental conditions of large Reynolds number TC flows.

## Acknowledgement

We thank J. Goodman for sharing his thoughts on angular momentum transport and boundary layers in our studies, and E. Schartman, E. Gilson, and P. Sloboda in helping to keep the experiments running smoothly. This work was supported by the U.S. Department of Energy, Fusion Energy Sciences under contract DE-AC02-09CH11466 through the Center for Momentum Transport & Flow Organization in Plasmas and Magnetofluids (CMTFO).

## References

- [1] A. Adams, P. M. Chesler, and H Liu. Holographic Turbulence. *Phys. Rev. Lett.*, 112:151602, 2014.
- [2] F. Carrasco, L. Lehner, R. C. Myers, O. Reula, and A. Singh. Turbulent flows for relativistic conformal fluids in 2+1 dimensions. *Phys. Rev. D*, 86:126006, 2012.
- [3] J. E. Rice, J. W. Hughes, P. H. Diamond, Y. Kosuga, Y. A. Podpaly, M. L. Reinke, M. J. Greenwald, Ö. D. Gürçan, T. S. Hahm, A. E. Hubbard, E. S. Marmor, C. J. McDevitt, and D. G. Whyte. Edge temperature gradient as intrinsic rotation drive in alcator *c*-mod tokamak plasmas. *Phys. Rev. Lett.*, 106:215001, 2011.
- [4] O. D. Gürcan, P. H. Diamond, C. J. McDevitt, and T. S. Hahm. A simple model of intrinsic rotation in high confinement regime tokamak plasmas. *Phys. Plasmas*, 17:032509, 2010.
- [5] H. Ji, M. Burin, E. Scharfman, and J. Goodman. Hydrodynamic turbulence cannot transport angular momentum effectively in astrophysical disks. *Nature*, 444:343, 2006.
- [6] E. Scharfman, H. Ji, M. Burin, and J. Goodman. Stability of quasi-Keplerian shear flow in a laboratory experiment. *Astron. Astrophys.*, 543:A94, 2012.
- [7] E. M. Edlund and H. Ji. Nonlinear stability of laboratory quasi-keplerian flows. *Phys. Rev. E*, 89:021004, 2014.
- [8] M. S. Paoletti and D. P. Lathrop. Angular momentum transport in turbulent flow between independently rotating cylinders. *Phys. Rev. Lett.*, 106:024501, 2011.
- [9] M. Seilmeyer, V. Galindo, G. Gerbeth, T. Gundrum, F. Stefani, M. Gellert, G. Rüdiger, M. Schultz, and R. Hollerbach. Experimental evidence for magnetorotational instability in a taylor-couette flow under the influence of a helical magnetic field. *Phys. Rev. Lett.*, 113:024505, 2014S.
- [10] F. Stefani, T. Gundrum, G. Gerbeth, G. Rüdiger, M. Schultz, J. Szklarski, and R. Hollerbach. Experimental evidence for magnetorotational instability in a taylor-couette flow under the influence of a helical magnetic field. *Phys. Rev. Lett.*, 97:184502, 2006.
- [11] D. R. Sisan, N. Mujica, W. A. Tillotson, Y. Huang, W. Dorland, A. B. Hassam, T. M. Antonsen, and D. P. Lathrop. Experimental observation and characterization of the magnetorotational instability. *Phys. Rev. Lett.*, 93:114502, 2004.
- [12] A. H. Roach, E. J. Spence, C. Gissinger, E. M. Edlund, P. Sloboda, J. Goodman, and H. Ji. Observation of a Free-Shercliff-Layer Instability in Cylindrical Geometry. *Phys. Rev. Lett.*, 108:154502, 2012.
- [13] E. J. Spence, A. H. Roach, E. M. Edlund, P. Sloboda, and H. Ji. Free magnetohydrodynamic shear layers in the presence of rotation and magnetic field. *Phys. Plasmas*, 19:056502, 2012.
- [14] R. Ostilla-Mónico, R. Verzicco, S. Grossman, and D. Lohse. Free magnetohydrodynamic shear layers in the presence of rotation and magnetic field. *J. Fluid Mech.*, 748:R3, 2014.
- [15] S. Maretzke, B. Hof, and M. Avila. Free magnetohydrodynamic shear layers in the presence of rotation and magnetic field. *J. Fluid Mech.*, 742:254, 2014.

- [16] D. S. Zimmerman, S. Andrés Triana, and D. P. Lathrop. Free magnetohydrodynamic shear layers in the presence of rotation and magnetic field. *Phys. Fluids*, 23:065104, 2011.
- [17] S. G. Huisman, R. C. A. van der Veen, C. Sun, and D. Lohse. Free magnetohydrodynamic shear layers in the presence of rotation and magnetic field. *Nature Commun.*, 5:3820, 2014.
- [18] G. Lesur, and P.-Y. Longaretti. Free magnetohydrodynamic shear layers in the presence of rotation and magnetic field. *Astron. Astrophys.*, 444:25, 2005.
- [19] M. Burin, H. Ji, E. Schartman, R. Cutler, P. Heitzenroeder, W. Liu, L. Morris, and S. Raftopolous. Reduction of Ekman circulation within Taylor-Couette flow. *Experiments in Fluids*, 40:962, 2006.
- [20] E. Schartman, H. Ji, and M. Burin. Development of a Couette-Taylor flow device with active minimization of secondary circulation. *Rev. Sci. Instrum.*, 80:024501, 2009.
- [21] F. Nordsiek, S. G. Huisman, R. C. A. van der Veen, C. Sun, D. Lohse, and D. P. Lathrop. Azimuthal velocity profiles in Rayleigh-stable Taylor-Couette flow and implied axial angular momentum transport. *J. Fluid Mech.*, 774:342, 2015.
- [22] D. A. Bennetts and L. M. Hocking. On nonlinear Ekman and Stewartson layers in a rotating fluid. *Proc. R. Soc. A.*, 333:469, 1973.
- [23] D. J. Baker. Shear layers in a rotating fluid. *J. Fluid Mech.*, 29:165, 1967.
- [24] K. Stewartson. On almost rigid rotations. *J. Fluid Mech.*, 3:17, 1957.
- [25] A. V. Obabko, F. Cattaneo, and P. F. Fischer. The influence of horizontal boundaries on Ekman circulation and angular momentum transport in a cylindrical annulus. *Phys. Scr.*, T132:014029, 2008.
- [26] O. Czarny, E. Serre, P. Bontoux, and R. Leuptow. Interaction between Ekman pumping and the centrifugal instability in Taylor-Couette flow. *Phys. Fluids*, 15:467, 2003.
- [27] M. Avila. Free magnetohydrodynamic shear layers in the presence of rotation and magnetic field. *Phys. Rev. Lett.*, 108:124501, 2012.
- [28] L. Shi, M. Rampp, B. Hof, and M. Avila. Free magnetohydrodynamic shear layers in the presence of rotation and magnetic field. *Comput. Fluids*, 106:1, 2015.